Laser-assisted photoemission from adsorbate-covered metal surfaces: Time-resolved core-hole relaxation dynamics from sideband profiles

C.-H. Zhang and U. Thumm
Department of Physics, Kansas State University, Manhattan, Kansas 66506, USA
(Received 23 April 2009; published 21 September 2009)

Illumination of an adsorbate-covered metal surface with an xuv and a delayed ir laser pulse can result in sidebands in the photoelectron (PE) spectra. We present a theoretical model for the delay-dependent PE spectra and show how the relaxation dynamics of xuv-induced core-level holes in adsorbate atoms can be deduced from the temporal shift between sideband peaks in the spectra of secondary adsorbate (Auger) electrons and conduction-band PEs from the substrate. Furthermore, in comparison with gaseous targets, we find a characteristic sideband-intensity enhancement in the laser-assisted photoemission from the substrate core-level bands. This sideband enhancement effect can be tested in experiments with tunable xuv wavelength. Our calculated PE spectra support time-resolved experiments for Xe-covered Pt(111) surfaces, promoting the direct analysis in the time domain of surface dynamical processes.

DOI: 10.1103/PhysRevA.80.032902 PACS number(s): 32.80.Hd, 42.65.Re, 79.60.Dp, 42.50.Hz

I. INTRODUCTION

During the past ten years, the development of intense ultrashort ir laser pulses was complemented by the generation of xuv pulses from higher harmonics of the primary ir pulses [1]. The synchronized combination of xuv and ir pulses in pump-probe experiments was first applied to resolve in time the relaxation of excited atoms [2] and subsequently to the time-dependent investigation with a resolution of ≈ 100 as $=10^{-16}$ s of electronic processes in atoms [3,4], molecules [5], and on surfaces [6–10]. The ability to follow the electron transfer and relaxation dynamics on solid surfaces in time advances both, basic research on fast electronic and plasmonic [8] interactions and applications in surface chemistry, photovoltaic energy conversion, and future nanoscopic devices with tunable electronic properties.

Depending on the length τ_X of the xuv pump pulse relative to the carrier period T_L of the ir probe pulse, dynamical information in photoelectron (PE) spectra is encoded either in the pump-probe-delay-dependent streaking [2,7,11,12] of the emitted PE energies or in the sideband structure of the PE spectrum [2,9]. For $\tau_X \ll T_L$, the energy of the xuv-emitted PEs electrons oscillates with period T_L as a function of the pump-probe delay τ. By measuring the relative temporal shift of the streaking oscillation in the τ-dependent PE spectra between electrons emitted by a short xuv pulse from $4f$ core levels (CLs) and the conduction band (CB) of a W(100) surface, Cavalieri *et al.* [7] recently obtained a delay of ≈ 100 as between the detection of core level and CB PEs, in agreement with quantum-mechanical calculations [12].

In contrast, for $\tau_X \gtrsim T_L$, PEs are continuously released during T_L such that the T_L-periodic streaking pattern is replaced by a satellite structure in the PE spectra [11,13]. This structure consists of a main photoemission peak at the nominal kinetic energy of the PE and a series of sideband peaks that are displaced by integer multiples (n) of the ir photon energy from the main peak. Sideband peaks occur on either side of the main peak and quickly decrease in amplitude as n increases. The change in the sideband intensities with τ encodes temporal information. Miaja-Avila *et al.* [9] recently measured such sideband spectra on a Xe-covered Pt(111) surface and extracted temporal information by analyzing their PE spectra within a heuristic model. By comparing the first ($n=1$) sideband intensities of xuv-emitted PEs from the CB of the Pt substrate and of Auger electrons (AEs) emitted from the Xe adsorbates in response to their xuv-induced inner-shell ionization, the authors deduced the lifetime $\tau_h = 7.1$ fs for the $4d^{-1}$ adsorbate core hole, in fair agreement with 6.3 fs derived from the spectral width in a previous energy-domain measurement [14].

In this paper, we discuss sideband structures in the PE and Auger-electron spectra from adsorbate-covered metal surfaces within a quantum-mechanical model for direct photoemission from the substrate and core-hole creation and decay in the adsorbate (Fig. 1). By illuminating the adsorbate-covered surface with overlapping synchronized xuv and ir pulses, electrons are photoemitted by absorption of a single xuv photon from localized core levels and delocalized states of the substrate. In all numerical applications, we assume

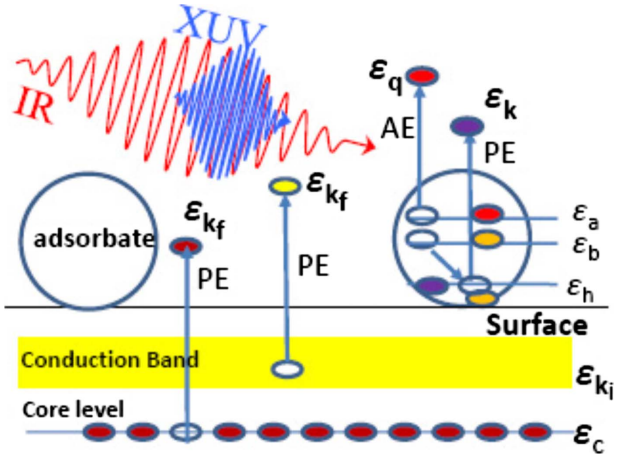

FIG. 1. (Color online) Sketch of the emission of substrate (core level and CB) and adsorbate (core level and Auger) electrons by an xuv pulse. Photoreleased electrons are exposed to a weak-delayed ir pulse. The xuv pulse length is on the order of or longer than the ir carrier period, leading to sidebands in the PE spectra.

grazingly incident laser pulses that are linearly polarized perpendicular to the surface and electron emission normal to the surface. Core-hole states created by xuv-inner-shell ionization decay by the delayed emission of Auger electrons [15]. Within this model, we reproduce sideband structures that were previously deduced from measured PE spectra from a Xe-covered Pt(111)surface in a proof-of-principle experiment [9]. Compared to photoemission from gaseous atoms, our model predicts that sideband intensities in the photoemission from substrate core levels are enhanced due to interfering PEs from different layers in the substrate, indicating that the sideband intensity encodes information on the transport of PEs in the solid. Unless stated otherwise, we use atomic units with $\hbar$, electron mass, elementary charge, and Bohr radius being equal to 1.

II. MODEL

A. Direct photoemission

In our model, absorption of a single xuv photon emits an electron from an initial Bloch state $\Psi_{\mathbf{k}_i}(\mathbf{r},t)=\Psi_{\mathbf{k}_i}(\mathbf{r})e^{-i\varepsilon_{\mathbf{k}_i}t}$ (with crystal momentum $\mathbf{k}_i$ and energy $\varepsilon_{\mathbf{k}_i}$) to an ir field-dressed final continuum state $\Psi_f(\mathbf{r},t)$. The photoemission transition amplitude in the dipole-length gauge for the perturbative interaction with the xuv electric field $\mathbf{E}_X(t)$ is

$$T_{\mathbf{k}_f,\mathbf{k}_i}(\tau)=\frac{1}{i}\int_{-\infty}^{+\infty}dt\langle\Psi_f(\mathbf{r},t)|zE_X(t+\tau)|\Psi_{\mathbf{k}_i}(\mathbf{r},t)\rangle, \quad (1)$$

where τ is the time delay between the ir and xuv pulses. The nonperturbative interaction of the released PE with the ir field $\mathbf{E}_L(t)$ is taken into account in strong-field approximation [11,12,16] by representing the final state $\Psi_f(\mathbf{r},t)$ as a damped Volkov wave function

$$\Psi_{\mathbf{k}_f}(\mathbf{r},t)=\Psi^V_{\mathbf{k}_f}(\mathbf{r},t)[\Theta(z)+e^{\kappa z}\Theta(-z)], \quad (2)$$

where $\Theta(z)$ is the unit step function, and $\Psi^V_{\mathbf{k}_f}(\mathbf{r},t)$ is the usual Volkov wave function

$$\Psi^V_{\mathbf{k}_f}(\mathbf{r},t)=\frac{1}{(2\pi)^{3/2}}e^{i[\mathbf{k}_f+\mathbf{A}(t)]\cdot\mathbf{r}}e^{i\phi_{\mathbf{k}_f}(t)-i\varepsilon_{\mathbf{k}_f}t}, \quad (3)$$

with kinetic momentum $\mathbf{k}_f$, energy $\varepsilon_{\mathbf{k}_f}=\mathbf{k}_f^2/2$, Volkov phase

$$\phi_{\mathbf{k}_f}=\frac{1}{2}\int_t^\infty dt_1[2\mathbf{k}_f\cdot\mathbf{A}_L(t_1)+\mathbf{A}_L^2(t_1)], \quad (4)$$

and vector potential

$$\mathbf{A}_L(t)=\int_t^\infty dt_1\mathbf{E}_L(t_1). \quad (5)$$

The damping factor $e^{\kappa z}$ in the final state (2) accounts for the finite mean-free path $\lambda=1/2\kappa$ of PEs inside the solid [17,18].

The photoemission probability is

$$P(\mathbf{k}_f;\tau)=\int d\mathbf{k}_i|T_{\mathbf{k}_f,\mathbf{k}_i}(\tau)|^2$$
$$=\int d\mathbf{k}_i\left|\int dtE_X(t)d_{\mathbf{k}_i,\mathbf{p}}e^{i(\varepsilon_{\mathbf{k}_f}-\varepsilon_{\mathbf{k}_i})t-i\phi_{\mathbf{k}_f}(t_d)}\right|^2, \quad (6)$$

where $t_d=t-\tau$ and $\mathbf{p}=\mathbf{k}_f+\mathbf{A}(t_d)$ is the canonical momentum in the ir field, and $d_{\mathbf{k}_i,\mathbf{p}}$ is the dipole matrix element (DME)

$$d_{\mathbf{k}_i,\mathbf{p}}=\frac{1}{(2\pi)^{3/2}}\int d\mathbf{r}e^{i\mathbf{p}\cdot\mathbf{r}}[\Theta(z)+e^{\kappa z}\Theta(-z)]z\Psi_{\mathbf{k}_i}(\mathbf{r}). \quad (7)$$

The integral over $\mathbf{k}_i$ in Eq. (6) is limited by the Fermi surface for CB electrons and to the first Brillouin zone ($|\mathbf{k}_i|<k_B=\pi/a$, a is the interlayer distance in the direction normal to the surface) for the CL electrons.

The initial state $\Psi_{\mathbf{k}_i}$ is composed of (i) incident and reflected Bloch waves, $\Psi^-_{\mathbf{k}_i}$ and $\Psi^+_{\mathbf{k}_i}$, that describe the motion of an electron inside the solid toward and away from the surface with crystal momenta $\mathbf{k}_i^\pm=(\mathbf{k}_{i,\parallel},\pm k_{i,z})$, and (ii) a transmitted part that represents the exponential decay of the initial-state's probability density into the vacuum ($z>0$) whose contribution to the transition probability is negligible.

For the delocalized initial CB state, we use the jellium approximation in which the potential of the semi-infinite metal is modeled by [19]

$$U(\mathbf{r})=-U_0\Theta(-z), \quad (8)$$

with $U_0=\varepsilon_F+W$, the Fermi energy ε_F, and work function W. The initial CB wave function can then be written as [11,20]

$$\Psi^{CB}_{\mathbf{k}_i}(\mathbf{r},t)=\frac{e^{-i\varepsilon_{\mathbf{k}_i}t}}{(2\pi)^{3/2}}e^{i\mathbf{k}_{i,\parallel}\cdot\mathbf{r}_\parallel}(e^{ik_{i,z}z}+Re^{-ik_{i,z}z}), \quad (9)$$

with $\varepsilon_{\mathbf{k}_i}=\mathbf{k}_i^2/2-U_0$, $R=(k_{i,z}-i\gamma)/(k_{i,z}+i\gamma)$, and $\gamma=\sqrt{2U_0-k_{i,z}^2}$. We have neglected the transmitted part. The corresponding DME is

$$d^{CB}_{\mathbf{k}_i,\mathbf{p}}=\frac{1}{(2\pi)^3}\left[\frac{\delta(\mathbf{p}_\parallel-\mathbf{k}_{i,\parallel})}{[p_z-k_{i,z}+i\kappa]^2}+\frac{\delta(\mathbf{p}_\parallel-\mathbf{k}_{i,\parallel})R}{[p_z+k_{i,z}+i\kappa]^2}\right]. \quad (10)$$

Substituting Eq. (10) into Eq. (6) and using $[\delta(\mathbf{p}_\parallel-\mathbf{k}_{i,\parallel})]^2=A\delta(\mathbf{p}_\parallel-\mathbf{k}_{i,\parallel})/(2\pi)^2$, where A is the area of the metal surface [21], we find the photoemission probability per unit area from the CB, including a factor of 2 for the spin orientations,

$$\frac{P^{CB}(k_f;\tau)}{A}=\frac{2}{(2\pi)^8}\int_0^{k_F}dk_{i,z}\left|\int dte^{i(\varepsilon_{k_f}-\varepsilon_{k_{i,z}})t-i\phi_{k_f}(t_d)}E_X(t)\right.$$
$$\left.\times\left[\frac{1}{[p_z-k_{i,z}+i\kappa]^2}+\frac{R}{[p_z+k_{i,z}+i\kappa]^2}\right]\right|^2. \quad (11)$$

For photoemission from localized core states, we construct a zero-bandwidth tight-binding initial wave function by superimposing atomic CLs ψ_c with binding energy ε_c that are centered at the lattice points $\{\mathbf{R}_i\}$ of the substrate,

$$\Psi^\pm_{\mathbf{k}_i}(\mathbf{r},t)=\sum_j e^{i\mathbf{k}_i^\pm\cdot\mathbf{R}_j}\psi_c(\mathbf{r}-\mathbf{R}_j)e^{-i\varepsilon_c t}, \quad (12)$$

and obtain the DME

$$d^{CL}_{\mathbf{k}_i,\mathbf{p}} = i\,\delta(\mathbf{p}_\parallel - \mathbf{k}_\parallel)\frac{d}{dp_z}\{\tilde{\psi}_c(\mathbf{p})\Delta_{p_z,k_{i,z}}(\kappa)\}, \tag{13}$$

where $\tilde{\psi}_c(\mathbf{p})$ is the Fourier transform of $\psi_c(\mathbf{r})$. The structure factor $\Delta_{p_z,k_{i,z}}(\kappa)=\Delta^-_{p_z,k_{i,z}}(\kappa)-\Delta^+_{p_z,k_{i,z}}(\kappa)$, with

$$\Delta^{\pm}_{p_z,k_{i,z}}(\kappa) = \frac{1}{1-e^{i[p_z(t)\pm k_{i,z}+i\kappa]a}}, \tag{14}$$

includes interlayer interference effects in terms of a coherent sum over contributions to the photocurrent from substrate layers located within a distance $\approx\lambda$ from the surface [17,18].

We note that for $\Delta(p_z,k_{i,z},\kappa)=1$, Eq. (13) gives the DME for isolated atoms. This is equivalent to taking the limit $\lambda=1/(2\kappa)\to 0$ so that only CL electrons from the top layer of atoms contribute the photoemission spectrum. We also note that by replacing $\tilde{\psi}(\mathbf{p})\to 1$ and in the limit $(p_z\mp k_{i,z})a\ll 1$, we obtain Eq. (10) for photoemission from the CB. Furthermore, we point out that $\Delta(p_z,k_{i,z},\kappa)$ depends on the ir field through $p_z=k_f+A_L(t)$ and on κ.

We model $\psi_c(\mathbf{r})$ in terms of a hydrogenic ground-state wave function,

$$\psi_c(\mathbf{r}) = \frac{2Z^{3/2}}{\sqrt{4\pi}}e^{-Zr}, \tag{15}$$

where Z is the effective nuclear charge which is adjusted to give the correct experimental binding energy ε_c [18]. The Fourier transformation of $\psi_c(\mathbf{r})$ is

$$\tilde{\psi}_c(\mathbf{p}) = \frac{2\sqrt{2}Z^{5/2}}{\pi}\frac{1}{[Z^2+\mathbf{p}^2]^2}. \tag{16}$$

This implies

$$d^{CL}_{\mathbf{k}_i,\mathbf{p}} = \frac{2\sqrt{2}Z^{5/2}\delta(\mathbf{p}_\parallel-\mathbf{k}_\parallel)}{\pi}\left\{\frac{a}{(Z^2+\mathbf{p}^2)^2}\left[\frac{e^{i[p_z-k_{i,z}+i\kappa]a}}{[1-e^{i[p_z-k_{i,z}+i\kappa]a}]^2} - \frac{e^{i[p_z+k_{i,z}+i\kappa]a}}{[1-e^{i[p_z+k_{i,z}+i\kappa]a}]^2}\right] - \frac{4ip_z\Delta_{p_z,k_{i,z}}(\kappa)}{(Z^2+\mathbf{p}^2)^3}\right\}. \tag{17}$$

The transition probability per unit area from CLs is obtained by inserting Eq. (17) into Eq. (6),

$$\frac{P^{CL}(k_f;\tau)}{A} = \frac{4Z^5}{\pi^4}\int_0^{k_B} dk_{i,z}\left|\int dt e^{i(\varepsilon_{k_f}-\varepsilon_c)t-i\phi_{k_f}(t_d)}E_X(t)\right. \times\left\{\frac{a}{[Z^2+p_z^2(t_d)]^2}\left[\frac{e^{i[p_z(t_d)-k_{i,z}+i\kappa]a}}{[1-e^{i[p_z(t_d)-k_{i,z}+i\kappa]a}]^2} - \frac{e^{i[p_z(t_d)+k_{i,z}+i\kappa]a}}{[1-e^{i[p_z(t_d)+k_{i,z}+i\kappa]a}]^2}\right]\right. \left.\left. - \frac{4ip_z(t_d)\Delta_{p_z(t_d),k_{iz}}(\kappa)}{[Z^2+p_z^2(t_d)]^3}\right\}\right|^2. \tag{18}$$

B. Photoemission followed by Auger relaxation

The coherent description of core-hole creation by the xuv-inner-shell ionization in isolated atoms and their subsequent relaxation by the emission of AEs was previously found to yield broader Auger spectra [15] than the incoherent addition of sequential inner-shell ionization and Auger decay [2]. The coherent quantum-mechanical modeling of these two processes, xuv photoemission of the adsorbate and its subsequent Auger relaxation, involves three bound and two continuum single-particle states, given by the core-hole level Ψ_h, two excited adsorbate levels Ψ_a and Ψ_b, and the continuum states of the emitted PE and AE, $\Psi_{\mathbf{k}}$ and $\Psi_{\mathbf{q}}$, respectively. The bound single-particle states Ψ_i, $i=h$, a, and b are eigenstates of the atomic Hamiltonian H_{at} with binding energies ε_i. Neglecting Coulomb interactions, the continuum states $\Psi_{\mathbf{s}}$, with momenta $\mathbf{s}=\mathbf{k}$, $\mathbf{q}$, are approximated in strong-field approximation as Volkov states with energies $\varepsilon_{\mathbf{s}}$.

Disregarding configuration interactions in the initial and final states, we define the three relevant channels for the adsorbate core ionization followed by Auger-relaxation process by antisymmetrized products of single-particle states for the ground state $|\Psi_h,\Psi_a,\Psi_b\rangle$, the CL photoemission channel $|\Psi_{\mathbf{k}},\Psi_a,\Psi_b\rangle$, and the final channel after relaxation of the adsorbate $|\Psi_{\mathbf{k}},\Psi_h,\Psi_{\mathbf{q}}\rangle$. Following [15], we expand the adsorbate state

$$|\Phi(t)\rangle = |\Psi_h,\Psi_a,\Psi_b\rangle + \int d\mathbf{k} b_{\mathbf{k}}(t)|\Psi_{\mathbf{k}},\Psi_a,\Psi_b\rangle + \int d\mathbf{k}d\mathbf{q} c_{\mathbf{k},\mathbf{q}}(t)|\Psi_{\mathbf{k}},\Psi_h,\Psi_{\mathbf{q}}\rangle \tag{19}$$

in these three channels, assuming sufficiently weak xuv (and ir) pulse intensities such that depletion of the initial channel is irrelevant. We determine the coefficients $b(\mathbf{k},t)$ and $c(\mathbf{k},\mathbf{q},t)$ by solving the time-dependent Schrödinger equation for $|\Phi(t)\rangle$ with the Hamiltonian

$$\hat{H}(t) = \sum_i H_{at}(i) + \frac{1}{2}\sum_{i\neq j} V(\mathbf{r}_i-\mathbf{r}_j) + V_E(\mathbf{r},t), \tag{20}$$

where

$$V_E(\mathbf{r},t) = \sum_i [\mathbf{E}_L(t)+\mathbf{E}_X(t+\tau)]\cdot\mathbf{r}_i \tag{21}$$

and $V(\mathbf{r}_i-\mathbf{r}_j)$ is the Coulomb potential between electrons i and j. Neglecting all Coulomb-pair interactions between single-particle states, except for the interaction $V_{\mathbf{q}}=\langle\psi_a\psi_b|V|\psi_h\psi_{\mathbf{q}}\rangle$ between Ψ_a and Ψ_b that drives the Auger decay, and using $\Psi_i(\mathbf{r},t)=\psi_i(\mathbf{r})e^{-i\varepsilon_i t}$, $i=h$, a, b, $\mathbf{k}$, and $\mathbf{q}$, we obtain the coupled equations

$$i\partial_t b_{\mathbf{k}}(t) = \mathbf{E}_X(t+\tau)\cdot\mathbf{d}^{CL}_{h,\mathbf{p}(t)}e^{i(\varepsilon_{\mathbf{k}}+\varepsilon_h)t-i\phi_{\mathbf{k}}(t)} + \int d\mathbf{q} V_{\tilde{\mathbf{q}}(t)}c_{\mathbf{k},\mathbf{q}}(t)e^{i(W_A-\varepsilon_{\mathbf{q}})t+i\phi_{\mathbf{q}}(t)}, \tag{22}$$

$$i\partial_t c_{\mathbf{k},\mathbf{q}}(t) = V^*_{\tilde{\mathbf{q}}(t)}b_{\mathbf{k}}(t)e^{-i(W_A-\varepsilon_{\mathbf{q}})t-i\phi_{\mathbf{q}}(t)}, \tag{23}$$

where $d^{CL}_{h,\mathbf{p}(t)}$ is the DME between the core-hole state and final Volkov state $\mathbf{p}(t)=\mathbf{k}+\mathbf{A}_L(t)$, $\tilde{\mathbf{q}}(t)=\mathbf{q}+\mathbf{A}_L(t)$, and $W_A=\varepsilon_a+\varepsilon_b-\varepsilon_h$. The first and second terms on the right-hand side of Eq. (22) describe the core-hole creation by the xuv

pulse and Auger relaxation, respectively. Integrating Eq. (23) and substituting

$$c(\mathbf{q},\mathbf{k},t) = -i\int_{-\infty}^{t} dt' V^{*}_{\tilde{\mathbf{q}}(t)} b(\mathbf{k},t') e^{-i(W_A-\varepsilon_{\mathbf{q}})t'-i\phi_{\mathbf{q}}(t')}, \quad (24)$$

into Eq. (22), we find

$$i\frac{db(\mathbf{k},t)}{dt} = \mathbf{E}(t)\cdot\mathbf{d}^{CL}_{h,\mathbf{p}(t)} e^{i(\varepsilon_{\mathbf{k}}+\varepsilon_h)t-i\phi_{\mathbf{k}}(t)} - i\int d\mathbf{q} V_{\tilde{\mathbf{q}}(t)} e^{-i(\varepsilon_{\mathbf{q}}-W_A)t+i\phi_{\mathbf{q}}(t)} \int_{-\infty}^{t} dt' V^{*}_{\tilde{\mathbf{q}}(t)} b(\mathbf{k},t') \times e^{-i(W_A-\varepsilon_{\mathbf{q}})t'-i\phi_{\mathbf{q}}(t')}. \quad (25)$$

The last term of this equation is nonlocal in time due to the interaction between PE and AE. By approximating

$$\int_{-\infty}^{t} dt' V^{*}_{\tilde{\mathbf{q}}(t)} b(\mathbf{k},t') e^{-i(W_A-\varepsilon_{\mathbf{q}})t'-i\phi_{\mathbf{q}}(t')} \approx V^{*}_{\tilde{\mathbf{q}}(t)} b(\mathbf{k},t) e^{-i\phi_{\mathbf{q}}(t)} \int_{-\infty}^{t} dt' e^{-i(W_A-\varepsilon_{\mathbf{q}})t'} = V^{*}_{\tilde{\mathbf{q}}(t)} b(\mathbf{k},t) e^{-i(W_A-\varepsilon_{\mathbf{q}})t-i\phi_{\mathbf{q}}(t)} \frac{1}{i(\varepsilon_{\mathbf{q}}-W_A-i\eta)}, \quad (26)$$

i.e., by neglecting the "memory" of $b(\mathbf{k},t')$, integration of Eq. (25) yields the closed form

$$b(\mathbf{k},t) = -i\int_{-\infty}^{t} dt' e^{-\Gamma(t-t')/2} e^{i(\varepsilon_{\mathbf{k}}+\varepsilon_h)t'-i\phi_{\mathbf{k}}(t')} \mathbf{E}(t'+\tau)\cdot\mathbf{d}^{CL}_{h,\mathbf{p}(t)}. \quad (27)$$

In this expression, we have neglected the energy shift

$$\Delta = -\mathrm{P}\int d\mathbf{q} \frac{|V_{\tilde{\mathbf{q}}(t)}|^2}{\varepsilon_{\mathbf{q}}-W_A} \quad (28)$$

of the PEs. For the remainder of this work, we will treat the core-hole decay rate

$$\Gamma = 2\pi\int d\mathbf{q} |V_{\tilde{\mathbf{q}}(t)}|^2 \delta(\varepsilon_{\mathbf{q}}-W_A) \quad (29)$$

as an adjustable parameter. Inserting Eq. (27) into Eq. (24), we obtain the amplitude for the coherent emission of PEs and AEs

$$c(\mathbf{k},\mathbf{q},t) = \int_{-\infty}^{t} dt' V^{*}_{\tilde{\mathbf{q}}(t)} e^{-i(W_A-\varepsilon_{\mathbf{q}})t'-i\phi_{\mathbf{q}}(t')} \int_{-\infty}^{t'} dt'' e^{-\Gamma(t'-t'')/2} \times e^{+i(\varepsilon_h+\varepsilon_{\mathbf{k}})t''-i\phi_{\mathbf{k}}(t'')} \mathbf{E}_X(t''+\tau)\cdot\mathbf{d}^{CL}_{h,\mathbf{p}(t)}, \quad (30)$$

which leads to the probability $P^{PE+AE}(\mathbf{k},\mathbf{q};\tau) = |c_{\mathbf{k},\mathbf{q}}(t\to\infty)|^2$ for the emission of PEs and AEs from the adsorbate with momenta $\mathbf{k}$ and $\mathbf{q}$,

$$P^{PE+AE}(\mathbf{k},\mathbf{q};\tau) = \left| \int_{-\infty}^{+\infty} dt V^{*}_{\tilde{\mathbf{q}}(t)} e^{i(\varepsilon_{\mathbf{q}}-W_A)t-i\phi_{\mathbf{q}}(t)} \int_{-\infty}^{t} dt' e^{\Gamma/2(t'-t)} \times e^{i(\varepsilon_h+\varepsilon_{\mathbf{k}})t'-i\phi_{\mathbf{k}}(t')} \mathbf{E}_X(t'+\tau)\cdot\mathbf{d}^{CL}_{h,\mathbf{p}(t)} \right|^2. \quad (31)$$

III. RESULTS

We assume ir and soft xuv laser electric field pulses

$$E_{L(X)}(t) = E_{L(X)0}(t)\cos(\omega_{L(X)}t), \quad (32)$$

with Gaussian envelopes

$$E_{L(X)0}(t) = E_{L(X)0} e^{-2\ln 2(t/\tau_{L(X)})^2}. \quad (33)$$

We use the experimental pulse lengths (full width at half maximum) τ_L=35.5 fs (τ_X=5.5 fs) and central frequencies ω_L=1.6 eV/$\hbar$ (ω_X=91 eV/$\hbar$) [9]. Using an ir peak intensity $I_L = 7\times10^{10}$ W/cm^2 of about 1/2 of the experimental peak intensity, we approximately take into account the effect of variable peak intensities inside the experimental focal volume. We model adsorbate core-hole decay in terms of an adjustable (Auger) rate Γ. The vector potential of the ir field is calculated in the slowly varying envelope approximation

$$A_L(t) = -\frac{E_{L0}(t)}{\omega_L}\sin(\omega_L t). \quad (34)$$

For weak ir fields, we obtain a Gaussian profile for the PE sideband spectra from CB,

$$P^{PE}_n(E;\tau) = \frac{I^{PE}_n(\tau)}{\sqrt{2\pi}\sigma^{PE}_n} e^{-(E-E_c-n\omega_L)^2/2(\sigma^{PE}_n)^2}, \quad (35)$$

with the intensity

$$I^{PE}_n(\tau) = I^{PE}_n(0) e^{-4\ln 2\tau^2/(\tau^{PE}_n)^2} \quad (36)$$

and the nominal kinetic energy $E_c=\omega_X-U_0$ of the PEs from the Fermi surface. The spectral and temporal widths are

$$\sigma^{PE}_n \approx \frac{1}{\tau_X}\sqrt{2\ln 2\left(1+\frac{n\tau_X^2}{\tau_L^2}\right)} \quad (37)$$

and

$$\tau^{PE}_n \approx \sqrt{\left(1+\frac{n\tau_X^2}{\tau_L^2}\right)}\frac{\tau_L}{\sqrt{n}}. \quad (38)$$

For photoemission followed by the Auger relaxation, sidebands appear in the coherent spectrum $P^{PE+AE}(\mathbf{q},\mathbf{k};\tau)$ (Fig. 2). The PE spectrum

$$P^{PE}(\mathbf{k};\tau) = \int d\mathbf{q} P^{PE+AE}(\mathbf{k},\mathbf{q};\tau) \quad (39)$$

is similar to that of the direct PEs from atoms.

Next, we direct our attention to the sideband structure of the AE spectrum

$$P^{AE}(\mathbf{q};\tau) = \int d\mathbf{k} P^{PE+AE}(\mathbf{k},\mathbf{q};\tau). \quad (40)$$

For weak ir fields and $\tau_L \gg 1/\Gamma$, we obtain a Lorentzian profile for the AE sideband spectra

$$P^{AE}_n(E;\tau) = \frac{I^{AE}_n(\tau)}{\pi}\frac{\sigma^{AE}_n/2}{(E-W_A+n\omega_L)^2+(\sigma^{AE}_n/2)^2}, \quad (41)$$

with an intensity

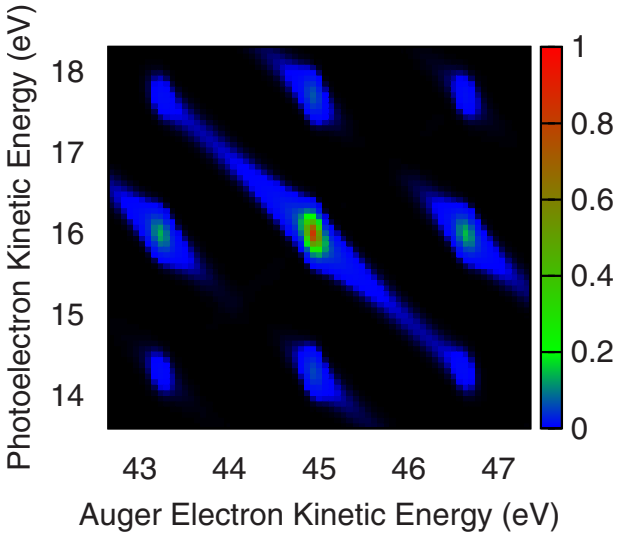

FIG. 2. (Color online) Sidebands in the spectrum of coherently emitted of PEs and AEs for no delay between xuv and ir pulse ($\tau=0$) and $\varepsilon_h=-75$ eV, $\varepsilon_a=\varepsilon_b=-15$ eV, and $\Gamma=0.14$ fs^{-1}. Laser and xuv parameters are given in the text.

$$I_n^{AE}(\tau) = I_n^{AE}(0)e^{-4\ln 2(\tau-\Delta\tau)^2/(\tau_n^{AE})^2}, \tag{42}$$

$\sigma_n^{AE}=\Gamma$, $\tau_n^{AE}=\tau_L/\sqrt{n}$, and $\Delta\tau=1/\Gamma$. This shows that, for long ir pulses, the lifetime of the core hole can be directly obtained according to $\tau_h=\Delta\tau$. Details of the derivation of the above results are given in Appendix A. In general, σ_n^{AE}, τ_n^{AE}, and $\Delta\tau$ depend on both Γ and τ_L. The numerical results in Fig. 3 for the first sideband peak in the AE spectrum illustrate the dependence of σ_1^{AE} and thus of P_1^{AE} on Γ and τ_L.

The graphs on the left side of Fig. 4 show our numerical results for $P^{PE(AE)}(E)$ in comparison with the experiment [9] at $\tau=0$. For direct photoemission from the Pt CB (top left graph), the line profiles assumed in [9] have the same functional (Gaussian) form (35) as predicted by our model, and the calculated widths $\sigma_1^{PE}=0.140$ eV and $\tau_1^{PE}=39$ fs agree with the experimental values 0.142 eV and 39 fs, respectively. However, for the energy dependence in the Xe NOO Auger spectra, the analysis in [9] assumed a Gaussian profile, in contrast to Eq. (41). Nevertheless, by adjusting $\Gamma=0.14$ fs^{-1}, our calculated intensities $I_{+1(-1)}^{AE}(0)=0.099$ (0.105) agree well with the corresponding experimental results 0.094 (0.102). The graphs on the right of Fig. 4 show experimental (top right graph) and corresponding calculated (bottom right graph) first sideband intensities as a function of τ. Our calculated temporal shift $\Delta\tau=7$ fs between the Pt CB and the Xe AEs agrees well with the experimental value of 6.2 fs. Interestingly, the observed $\Delta\tau=6.2$ fs indeed is close to $\tau_h=1/\Gamma=7.1$ fs.

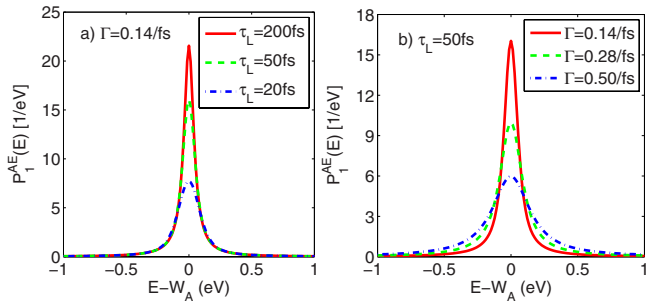

FIG. 3. (Color online) Auger-electron spectrum near the first sideband peak as a function of the ir pulse length τ_L (a) and the core-hole decay rate Γ (b). The sideband spectral widths depend on both τ_L and Γ.

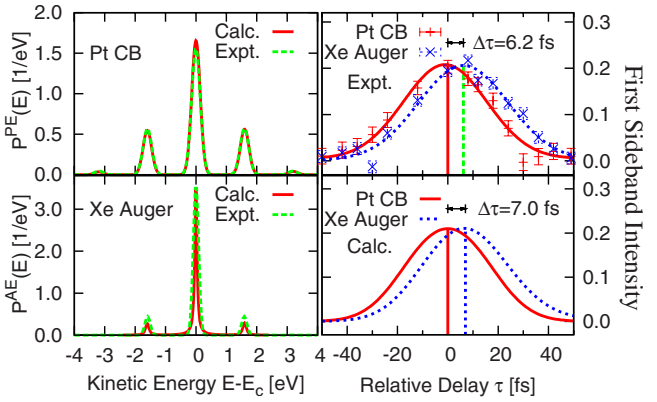

FIG. 4. (Color online) Theoretical and experimental [9] PE spectra for laser-assisted photoemission from a Xe/Pt(111) surface. Left: sideband intensities for no delay ($\tau=0$) between xuv and ir pulses for xuv-emitted Pt CB electrons from the Fermi level (top) and Xe AEs (bottom). Right: experimental (top) and calculated (bottom) first sideband intensities $I_{+1}^{PE}(\tau)$ and $I_{+1}^{AE}(\tau)$ for Pt CB electrons and Xe AEs, revealing a temporal shift $\Delta\tau$. Sideband intensities in the AE spectra are multiplied by a factor of 2.16.

The Gaussian spectral and temporal sideband profiles (35) and (36) for xuv-emitted PEs from delocalized Pt CB states confirm the choice of the response function in [9]. However, the Lorentzian profile (41) of the Auger sideband spectrum is in better agreement with the experimental data than the Gaussian form [22]. We find the best agreement with the experimental AE spectrum [9] for a core-hole-decay rate $\Gamma=0.14$ fs^{-1}. The dependence of the shift $\Delta\tau$ and temporal width τ_1^{AE} of the first sideband in the AE spectrum on Γ is shown in Fig. 5.

Sideband intensities might be used to explore the transport properties of core-level PEs inside the metal due to the

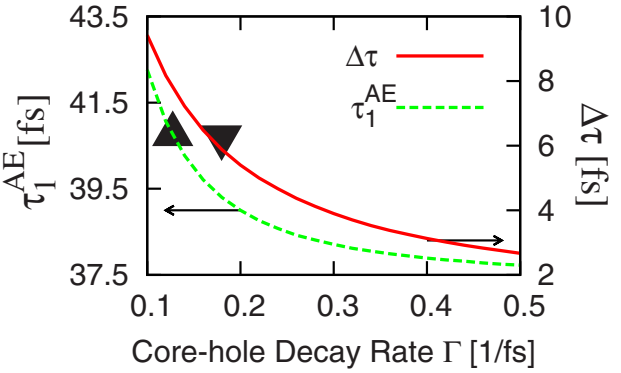

FIG. 5. (Color online) Temporal width τ_1^{AE} and shift $\Delta\tau$ of the first sideband intensity in adsorbate AE spectra as a function of the decay rate Γ. The symbols ▲ and ▼ indicate experimental values [9] for τ_1 and $\Delta\tau$.

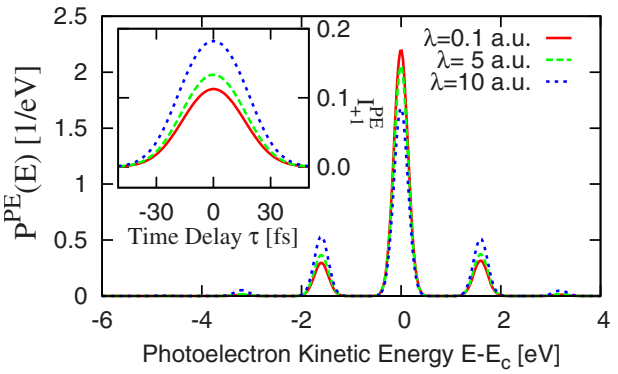

FIG. 6. (Color online) Sideband enhancement in the normalized PE spectrum of the $5p_{3/2}$ band in Pt. The main peak is centered at E_c=39.3 eV. Inset: first sideband intensity $I^{PE}_{+1}(\tau)$.

dependence of the DME (13) on the structure factor Δ, which coherently adds contributions to the net PE current from different layers. As shown in Fig. 6, Δ causes the redistribution of emission probability between the main peak and sideband peaks relative to photoemission from isolated atoms. This redistribution in the photoemission spectrum depends on λ, i.e., on the electron transport inside the solid. We verified numerically that for $\lambda < 0.1$, the profile of the sideband peaks equals the corresponding atomic case. However, as λ increases, the main peak gets depleted while the sidebands become enhanced. The derivation in Appendix B shows that for $\lambda \gtrsim a/2$, the dominant *n*th sideband amplitude in Eq. (6) for photoemission from CLs is approximately proportional to

$$e^{in\omega_L t} \sum_{l,m;l+m=n} J_l\left(\frac{kE_{L0}(t)}{\omega_L^2}\right) J_m\left(\frac{E_{L0}(t)a}{\omega_L}\right). \tag{43}$$

The Bessel expansion of the Volkov phase in $e^{i\phi_{\mathbf{k}}(t)}$ accounts for the discrete sideband structure in isolated-atom spectra (sum over *l*). In contrast, the sum over *m* in Eq. (43) originates in a Bessel expansion of the structure factor Δ. Note that the argument of Bessel function J_m depends on the interlayer spacing *a*. Both *l* and *m* combine to a given sideband order $n=l+m$. For $n \neq 0$ and for the laser parameters and electron momenta *k* considered in this work, all terms in Eq. (43) have the same sign, such that the sidebands intensities get constructively enhanced, while the main PE peak intensity decreases. We emphasize that Eq. (43) explains the origin of the sideband-intensity redistribution, but not the dependence of the sideband intensity on λ (see Appendix B for details).

IV. CONCLUSION AND OUTLOOK

In conclusion, by comparing the profiles of sideband peaks in xuv photoemission from localized atomic and delocalized metal CB levels with the spectrum of AEs emitted during the decay of a core hole, we analyzed (i) the relative delay of substrate PEs and adsorbate AEs in agreement with a recent experiment [9] and (ii) the sidebands profiles in PE and AE spectra in support of a previous analysis of measured PE spectra [9]. In addition, we found an intensity redistribution between the main and sideband peaks in core-level PE spectra from metal surfaces that is related to the transport of photoreleased electrons in the substrate. Since the transport (in our model λ) depends on the PE kinetic energy [19], and thus on ω_X, we anticipate future tests of this predicted sideband enhancement effect in experiments with tunable xuv wavelength.

We note that a factor of 0.5 is missing in the definition of κ in Ref. [12]. After correcting this factor, the adjusted value $\lambda=5$ reproduces the measured 110 as temporal shift [7]. This value for the mean-free path, however, lies below the universal curve [19]. A possible reason for this discrepancy is that in [12], we compare the centers of energy for the two limiting cases of photoemission from *completely* localized CLs and *completely* delocalized CB levels. While we believe fully localized states are a good approximation for the 4*f* state in tungsten, the fully delocalized plane-wave (jellium) approximation does not take into account that $5d\,6s$ CB states in tungsten have some localized character. For a fixed value of $\lambda=5$, allowing for partial localization of the conduction states decreases the temporal shift between core and CB levels. This decrease would be compensated by increasing λ to a value closer to the universal curve. More work is needed toward a more accurate description of (i) the metal conduction band as well as (ii) the propagation of PEs inside the solid [23].

ACKNOWLEDGMENTS

We thank Luis Miaja-Avila for providing the experimental data. This work was supported by the NSF and the Division of Chemical Sciences, Office of Basic Energy Sciences, Office of Energy Research, U.S. DOE.

APPENDIX A: DERIVATION OF Eqs. (35)–(42)

We assume the xuv and ir pulses given by Eq. (32). To simplify the notation, we define $\alpha_{X(L)}=2\ln 2/\tau^2_{X(L)}$. For photoemission from CB states inside a solid, the dependence of the DME on the vector potential $A_L(t)$ [see Eq. (10)] can be neglected. Expansion of the Volkov phase factor in Eq. (6),

$$e^{i\phi_{\mathbf{k}}(t)} = \sum_n e^{in\omega_L t} J_n[\mathbf{k}\cdot\mathbf{E}_{L0}(t)/\omega_L^2], \tag{A1}$$

leads to the photoemission amplitude in the direction normal to the surface

$$T_{i\to f}(\tau) = -id^{CB}_{\mathbf{k}_i,\mathbf{k}_f} E_{X0} \sum_n \int_{-\infty}^{+\infty} dt e^{-\alpha_X t^2} e^{i(\varepsilon_{\mathbf{k}_f}-\varepsilon_{\mathbf{k}_i}+n\omega_L-\omega_X)t} \times J_n\left[\frac{k_f E_{L0}(t-\tau)}{\omega_L^2}\right]. \tag{A2}$$

The spectrum without ir pulse is

$$P^{PE}_{xuv}(k_f) = |d^{CB}_{\mathbf{k}_i,\mathbf{k}_f} E_{X0}|^2 \frac{\pi}{\alpha_X} e^{-[(\varepsilon_{\mathbf{k}_f}-\varepsilon_{\mathbf{k}_i}-\omega_X)^2/4\alpha_X]}, \tag{A3}$$

and the total transition intensity is

$$I_{xuv}^{PE} = |d_{\mathbf{k}_i,\mathbf{k}_f}^{CB} E_{X0}|^2 \frac{2\pi^{3/2}}{\sqrt{\alpha_X}}. \tag{A4}$$

For weak ir fields, x is small, and we can approximate the nth order Bessel function

$$J_n(x) \approx \frac{1}{n!}\left(\frac{x}{2}\right)^n \tag{A5}$$

in order to obtain

$$\begin{aligned} T_{i\to f}(\tau) &= -id_{\mathbf{k}_i,\mathbf{k}_f}^{CB} E_{X0} \sum_n \frac{\varepsilon_{k_f}^{n/2} E_{L0}^n}{2^{n/2} n!\, \omega_L^{2n}} \int_{-\infty}^{+\infty} dt e^{-\alpha_X t^2 - n\alpha_L (t-\tau)^2} e^{i(\varepsilon_{\mathbf{k}_f} - \varepsilon_{\mathbf{k}_i} + n\omega_L - \omega_X)t} \\ &= -id_{\mathbf{k}_i,\mathbf{k}_f}^{CB} E_{X0} \sum_n \frac{\varepsilon_{k_f}^{n/2} E_{L0}^n}{2^{n/2} n!\, \omega_L^{2n}} \sqrt{\frac{\pi}{\alpha_X + n\alpha_L}} e^{-n\alpha_L \tau^2} e^{-[(\varepsilon_{\mathbf{k}_f} - \varepsilon_{\mathbf{k}_i} + n\omega_L - \omega_X - 2ni\alpha_L \tau)^2/4(\alpha_X + n\alpha_L)]}. \end{aligned} \tag{A6}$$

The profile of the nth sideband peak, divided by I_{xuv}^{PE}, is

$$P_n^{PE}(k_f;\tau) = I_n^{PE}(0) e^{-4\ln 2[\tau^2/(\tau_n^{PE})^2]} e^{-[(\varepsilon_{\mathbf{k}_f} - \varepsilon_{\mathbf{k}_i} + n\omega_L - \omega_X)^2/2(\sigma_n^{PE})^2]}, \tag{A7}$$

with

$$I_n^{PE}(0) = \frac{\varepsilon_{\mathbf{k}_f}^n E_{L0}^{2n}}{2^n (n!)^2 \omega_L^{4n}} \frac{1}{2\pi} \sqrt{\frac{\alpha_X}{\alpha_X + n\alpha_L}} \tag{A8}$$

and the spectral width σ_N^{PE} and temporal width τ_n^{PE} given by Eqs. (37) and (38).

In order to analyze the sideband profiles in the Auger-decay spectrum, we neglect the ir streaking of the PEs, such that

$$\mathbf{d}_{h,\mathbf{p}}^{CL} = \mathbf{d}_{h,\mathbf{k}}^{CL} = -i\frac{8\sqrt{2}Z^{5/2}}{\pi} \frac{\mathbf{k}}{(Z^2 + \mathbf{k}^2)^3}. \tag{A9}$$

Approximating the two-body matrix element $V_{\tilde{\mathbf{q}}(t)}^*$ in Eq. (31) as a constant V, and using

$$e^{-\alpha(t-\tau)^2} = \sqrt{\frac{\pi}{\alpha}} \int \frac{d\omega}{2\pi} e^{-\omega^2/4\alpha} e^{i\omega(t-\tau)}, \tag{A10}$$

we find for $\mathbf{q} \| \mathbf{E}_L$

$$P^{PE+AE}(\varepsilon_{\mathbf{q}}, \mathbf{k}; \tau) \approx \frac{\pi V^2}{\alpha_X} |\mathbf{E}_{X0} \cdot \mathbf{d}_{h,\mathbf{k}}^{CL}|^2 \left| \int \frac{d\omega}{2\pi} e^{-\omega^2/4\alpha_X} \sum_n \int_{-\infty}^{+\infty} dt J_n\left[\frac{qE_{L0}(t-\tau)}{\omega_L^2}\right] \frac{e^{i(\omega - E_c + \varepsilon_{\mathbf{k}} + n\omega_L + \varepsilon_{\mathbf{q}} - W_A)t}}{\omega - E_c + \varepsilon_{\mathbf{k}} - i\Gamma/2} \right|^2, \tag{A11}$$

where $E_c = \omega_X - |\varepsilon_h|$ is the central kinetic energy of the PEs. The Auger transition probability is then

$$P^{AE}(\varepsilon_{\mathbf{q}};\tau) = \int d\mathbf{k} P^{PE+AE}(\varepsilon_{\mathbf{q}}, \mathbf{k}; \tau) \approx \frac{C\pi}{\alpha_X} \int d\varepsilon_{\mathbf{k}} \left| \int \frac{d\omega}{2\pi} e^{-\omega^2/4\alpha_X} \sum_n \int_{-\infty}^{+\infty} dt J_n\left[\frac{pE_{L0}(t-\tau)}{\omega_L^2}\right] \frac{e^{i(\omega - E_c + \varepsilon_{\mathbf{k}} + n\omega_L + \varepsilon_{\mathbf{q}} - W_A)t}}{\omega - E_c + \varepsilon_{\mathbf{k}} - i\Gamma/2} \right|^2, \tag{A12}$$

where

$$C = \frac{1024 V^2 E_{X0}^2 Z^5}{3\pi} \frac{E_c^{3/2}}{(Z^2 + 2E_c)^6}. \tag{A13}$$

In particular, approximating $J_0(x) \approx 1$ for a weak ir pulse, we obtain for the main peak ($n=0$)

$$P_0^{AE}(\varepsilon_{\mathbf{q}}) \approx \sqrt{\frac{\pi}{2\alpha_X}} \frac{C}{\Gamma} \frac{1}{\pi} \frac{\Gamma/2}{(\varepsilon_{\mathbf{q}} - W_A)^2 + \Gamma^2/4}, \tag{A14}$$

which is a Lorentzian of width $\Gamma = \sigma_0$. Since Eq. (A14) does not include the depletion of the main peak caused by the ir field, it is identical to the Auger-decay probability without ir field. Without ir field, the total probability follows as

$$I_{xuv}^{AE} = \int d\varepsilon_{\mathbf{q}} P_0^{AE}(\varepsilon_{\mathbf{q}}) = \sqrt{\frac{\pi}{2\alpha_X}} \frac{C}{\Gamma}. \tag{A15}$$

For the sideband contribution to the spectrum ($n \neq 0$), we find after division by I_{xuv}^{AE}

$$P_n^{AE}(\varepsilon_{\mathbf{q}};\tau) = \frac{W_A^n E_{L0}^{2n}}{2^n (n!)^2 \omega_L^{4n}} \frac{\sqrt{\alpha_X}}{\sqrt{n\alpha_L + \alpha_X}} \frac{\Gamma}{8n\alpha_L} \times \left| W\left(\frac{\Delta E + i(\Gamma/2 - 2n\alpha_L \tau)}{2\sqrt{n\alpha_L}} \right) \right|^2 e^{-4n \ln 2(\tau/\tau_L)^2}, \tag{A16}$$

where $\Delta E = W_A - n\omega_L - \varepsilon_{\mathbf{q}}$, and where

$$W(z) = e^{-z^2} \mathrm{erfc}(-iz) \tag{A17}$$

is the so-called Faddeeva function, which is related to the complex error function erfc. For $\tau_L \gg 1/\Gamma$, the magnitude of the argument of the Faddeeva function becomes large. In the limit $|z| \to \infty$, the Faddeeva function becomes

$$W(z) \approx \frac{i}{\sqrt{\pi}} \frac{1}{z}. \tag{A18}$$

Therefore, near sideband centers ($\Delta E \sim 0$), we obtain the Lorentzian profile

$$P_n^{PE}(\varepsilon_{\mathbf{q}};\tau) \approx \frac{W_A^n E_{L0}^{2n}}{2^n (n!)^2 \omega_L^{4n}} \frac{\sqrt{\alpha_X}}{\sqrt{n\alpha_L + \alpha_X}} e^{-4 \ln 2(\tau - \Delta\tau/\tau_n)^2} \times \frac{1}{\pi} \frac{\sigma_n^{AE}/2}{(W_A - n\omega_L - \varepsilon_{\mathbf{q}})^2 + (\sigma_n^{AE})^2/4}, \tag{A19}$$

with $\sigma_n^{AE} = \Gamma$, $\Delta\tau = 1/\Gamma$, and $\tau_n = \tau_L/\sqrt{n}$. The corresponding intensity reads as

$$I_n^{AE}(\tau) = I_n^{AE}(0) e^{-4 \ln 2(\tau - \Delta\tau/\tau_n)^2}, \tag{A20}$$

with

$$I_n^{AE}(0) = \frac{W_A^n E_{L0}^{2n}}{2^n (n!)^2 \omega_L^{4n}} \frac{\sqrt{\alpha_X}}{\sqrt{n\alpha_L + \alpha_X}}. \tag{A21}$$

APPENDIX B: DERIVATION OF Eq. (43)

To understand the enhancement of the sideband intensity for photoemission from periodically distributed CLs relative to an atomic gas, we note that for $\lambda \gtrsim a/2$, the last term in the curly brackets and second term the straight brackets in Eq. (17) can be neglected. This is confirmed by our numerical tests and can also be seen analytically: the last term in the curly brackets in Eq. (17), $4ip_z \Delta_{p_z,k_{i,z}}(\kappa)(Z^2 + \mathbf{p}^2)^{-3}$, becomes negligible compared to the first term in curly brackets due to its much larger denominator $(Z^2 + \mathbf{p}^2)^3$. The second term in the straight brackets in Eq. (17), $e^{i[p_z + k_{i,z} + i\kappa]a}/[1 - e^{i[p_z + k_{i,z} + i\kappa]a}]^2$, can be neglected relative to the first term in straight brackets since (i) $k_{i,z} \geq 0$ and (ii) $p_z + k_{i,z} = k_{f,z} + A_L(t) + k_{i,z} > 0$, which for the considered ir laser intensity, leads to a rapidly oscillating exponential factor. We also verified that approximating $1/[1 - e^{i[k_{f,z} + A_L(t) - k_{i,z} + i\kappa]a}]^2 \approx 1$ does not significantly change Eq. (18). With these approximations, the probability per unit area for CL photoemission becomes

$$\frac{P^{CL}(k_f;\tau)}{A} \approx \frac{4Z^5 k_B}{\pi^4} e^{-a/\lambda} \left| \int dt e^{i(\varepsilon_{k_f} - \varepsilon_c)t - i\phi_{k_f}(t_d)} \times E_X(t) \frac{a}{[Z^2 + p_z^2(t_d)]^2} e^{iA_L(t_d)a} \right|^2. \tag{B1}$$

Expanding in terms of Bessel functions both, the phase

$$e^{iA_L(t_d)a} = \sum_m e^{im\omega_L t} J_m\left(\frac{E_{L0}(t_d)a}{\omega_L} \right) \tag{B2}$$

and the Volkov phase factor $e^{-i\phi_{k_f}(t_d)}$ in Eq. (B1), we find

$$\frac{P^{CL}(k_f;\tau)}{A} = \frac{4Z^5 k_B}{\pi^4} e^{-a/\lambda} \left| \int dt \frac{a e^{i(\varepsilon_{k_f} - \varepsilon_c)t} E_X(t)}{[Z^2 + p_z^2(t_d)]!^2} \sum_{l,m} e^{i(l+m)\omega_L t_d} \times J_l\left(\frac{kE_{L0}(t_d)}{\omega_L^2} \right) J_m\left(\frac{E_{L0}(t_d)a}{\omega_L} \right) \right|^2. \tag{B3}$$

Combing $l + m = n$, we see that this equation includes the nth sideband amplitudes for photoemission from substrate CLs inside the solid (43).

Note that all numerical results in this work are based on the full Eq. (18). We emphasize that Eqs. (B3) and (43) show the sideband enhancement, but not the dependence of this enhancement on λ. The actual amount of sideband enhancement at a given λ depends on the competition among all terms in Eq. (18) and is shown in Fig. 6.

[1] F. Krausz and M. Ivanov, Rev. Mod. Phys. **81**, 163 (2009).

[2] M. Drescher, M. Hentschel, R. Kienberger, M. Uiberacker, V. Yakovlev, A. Scrinzi, Th. Westerwalbesloh, U. Kleineberg, U. Heinzmann, and F. Krausz, Nature (London) **419**, 803 (2002).

[3] P. Johnsson, J. Mauritsson, T. Remetter, A. L'Huillier, and K. J. Schafer, Phys. Rev. Lett. **99**, 233001 (2007).

[4] M. Uiberacker, Th. Uphues, M. Schultze, A. J. Verhoef, V. Yakovlev, M. F. Kling, J. Rauschenberger, N. M. Kabachnik, H. Schröder, M. Lezius, K. L. Kompa, H.-G. Muller, M. J. J. Vrakking, S. Hendel, U. Kleineberg, U. Heinzmann, M. Drescher, and F. Krausz, Nature (London) **446**, 627 (2007).

[5] A. S. Sandhu, E. Gagnon, R. Santra, V. Sharma, W. Li, P. Ho, P. Ranitovic, C. L. Cocke, M. M. Murnane, and H. C. Kapteyn, Science **322**, 1081 (2008).

[6] L. Miaja-Avila, C. Lei, M. Aeschlimann, J. L. Gland, M. M. Murnane, H. C. Kapteyn, and G. Saathoff, Phys. Rev. Lett. **97**, 113604 (2006).

[7] A. L. Cavalieri, N. Müller, Th. Uphues, V. S. Yakovlev, A. Baltuška, B. Horvath, B. Schmidt, L. Blümel, R. Holzwarth, S. Hendel, M. Drescher, U. Kleineberg, P. M. Echenique, R. Kienberger, F. Krausz, and U. Heinzmann, Nature (London) **449**, 1029 (2007).

[8] M. I. Stockman, M. F. Kling, U. Kleineberg, and F. Krausz,

Nature Photon. **1**, 539 (2007).
[9] L. Miaja-Avila, G. Saathoff, S. Mathias, J. Yin, C. La-o-vorakiat, M. Bauer, M. Aeschlimann, M. M. Murnane, and H. C. Kapteyn, Phys. Rev. Lett. **101**, 046101 (2008).
[10] G. Saathoff, L. Miaja-Avila, M. Aeschlimann, M. M. Murnane, and H. C. Kapteyn, Phys. Rev. A **77**, 022903 (2008).
[11] J. C. Baggesen and L. B. Madsen, Phys. Rev. A **78**, 032903 (2008).
[12] C.-H. Zhang and U. Thumm, Phys. Rev. Lett. **102**, 123601 (2009).
[13] E. M. Kosik, L. Corner, A. S. Wyatt, E. Cormier, I. A. Walmsley, and L. F. Dimauro, J. Mod. Opt. **52**, 361 (2005).
[14] M. Jurvansuu, A. Kivimäki, and S. Aksela, Phys. Rev. A **64**, 012502 (2001).
[15] O. Smirnova, V. S. Yakovlev, and A. Scrinzi, Phys. Rev. Lett. **91**, 253001 (2003).
[16] M. Kitzler, N. Milosevic, A. Scrinzi, F. Krausz, and T. Brabec, Phys. Rev. Lett. **88**, 173904 (2002).
[17] P. J. Feibelman, Phys. Rev. B **10**, 4932 (1974).
[18] S. Hüfner, *Photoelectron Spectroscopy*, 3rd ed. (Springer-Verlag, Berlin, 2003).
[19] A. Zangwill, *Physics at Surfaces* (Cambridge University Press, New York, 1988).
[20] U. Thumm, J. Phys. B **25**, 421 (1992); P. Kürpick, U. Thumm, and U. Wille, Phys. Rev. A **56**, 543 (1997).
[21] F. H. M. Faisal, *Theory of Multiphoton Process* (Plenum Press, New York, 1987).
[22] Using Eq. (41), one can improve the fit to the measured xuv+ir AE spectrum in Ref. [9]; Miaja-Avila (private communication).
[23] C. Lemell, B. Solleder, K. Tökési, and J. Burgdörfer, Phys. Rev. A **79**, 062901 (2009).